Crystal growth and interface relaxation rates from fluctuations in an equilibrium simulation of the Lennard-Jones (100) crystal-melt system

H. L. Tepper[a] and W. J. Briels[b]
Computational Dispersion Rheology, University of Twente, P.O. Box 217, 7500 AE Enschede, The Netherlands

(Received 11 September 2001; accepted 28 December 2001)

The kinetic coefficient of crystallization is calculated according to a previously introduced equilibrium method [Phys. Rev. Lett. **79**, 5074 (1997)]. The existence of two regimes of interface relaxation and macroscopic growth, such as they were found in previous nonequilibrium simulations, is fully confirmed by the results of the equilibrium method. Special attention is given to the relation between pressure fluctuations and fluctuations of the amount of crystalline material. Furthermore, we investigate the density and order parameter profiles of the interface and make a clear distinction between the instantaneous structure and the time-averaged profile which is usually presented. © *2002 American Institute of Physics.* [DOI: 10.1063/1.1452110]

I. INTRODUCTION

Over the past few decades, molecular dynamics (MD) simulations have proved to be an extremely powerful tool in the study of crystal growth and melting processes.[1–3] Given the experimental difficulty in probing the interface between two dense phases, the atomistic details coming from MD methods have provided an excellent alternative in understanding the processes taking place at the interface.

Much information has been obtained on the structure (e.g., diffuseness, anisotropy) of various crystal-melt interfaces,[4–7] but on the dynamics of crystal growth from the melt there are still some open questions, even for the simplest model systems. As an example, concerning the growth and melting rates of atomic systems, there has been much debate on whether a slope discontinuity in the rates exists upon crossing the melting point. Such a singularity was claimed by Tymczak and Ray[8,9] in their study of crystallization and melting kinetics in sodium, in clear contradiction with earlier theoretical considerations.[10,11] In a preceding study of ours[12] we did a very accurate investigation of growth and melting rates of the Lennard-Jones FCC (100) surface close to equilibrium. From this we were able to rule out the possibility of a singularity at the melting point and argued that any such findings for similar systems must be due to an artifact of the simulation.

One of the main problems to get accurate dynamics data out of simulations of two-phase systems is that it is extremely difficult to ensure a properly prepared nonequilibrium interface. The crystalline surface induces order which extends far into the liquid, and dynamic correlation lengths are probably even much longer. In an earlier study[13] for instance, we found a clear slope discontinuity between crystallization and melting rates. This was shown to disappear with the incorporation of lattice imperfections in the crystal that were only obtained after proper equilibration.

In our previous paper[12] we found that when nonequilibrium growth simulations were started after extensive equilibration of the system at the melting point, considerable time was needed for the interface to relax to its nonequilibrium shape (i.e., the shape that corresponds to the circumstances of the experiment). We discovered two regimes of linear growth: a short-time regime associated with interface relaxation and a long-time regime associated with the macroscopic limit of growth and melting. We studied the influence of size effects and found that the second regime could only be measured accurately for sufficiently large systems (larger than mostly used in earlier simulations). In a system of $8.044\sigma\times 8.044\sigma\times 69.595\sigma$ (4048 atoms), the initial regime lasts much longer than in a system of $8.044\sigma\times 8.044\sigma\times 139.19\sigma$ (8096 atoms), which makes an accurate calculation of the long-time dynamics in the smaller system quite cumbersome. To sum up, in simulations where two phases are combined, it is of utmost importance to take large enough system sizes, equilibration times and run times, meaning generally much larger than in simulations of bulk systems.

In our 1997 paper[14] we introduced a method to extract the kinetic coefficient (i.e., the slope of the rates R versus temperature T) from fluctuations of the number of solid particles in one simulation at equilibrium. Apart from avoiding the computational cost of having to do numerous nonequilibrium simulations at a range of temperatures, this method has the advantage that the simulations can be carried out principally *ad infinitum*, providing as accurate statistics as one wishes. Unless special measures are taken against it, nonequilibrium simulations are limited to the time during which the whole box becomes crystalline or liquid. Given the enormous growth rates for atomic systems, this time can become unmanageably short even for moderate supersaturations.

It is the main goal of the present paper to investigate whether the equilibrium method gives accurate results for the system sizes of our previous nonequilibrium study (i.e., 4048 and 8096 atoms, respectively). In particular, we would like to find further evidence for the presence of two growth regimes.

[a]Electronic mail: Harald.Tepper@hec.utah.edu
[b]Electronic mail: w.j.briels@tn.utwente.nl

A second objective is to find a method to calculate the kinetic coefficient of normal growth exclusively using data from one and the same two-phase equilibrium simulation, where in our previous approach we needed external input to calculate this coefficient.

The paper is organized as follows. First we will briefly describe the model system and the way we carried out the equilibration. Then we will study the relation between number fluctuations and pressure fluctuations. We will suggest the substitution of a factor from the original derivation (containing equilibrium thermodynamic properties of the bulk phases) by a correlation factor which can be measured directly in the two-phase system. We will elaborate on this by considering the influence of fluctuations of the pressure that are not directly related to fluctuations of the amount of crystalline material. In the subsequent section, we will compare the prediction of the kinetic coefficient from the equilibrium method with the nonequilibrium data from the previous study and discuss the influence of system size on the accuracy. After this, we will describe in detail the structure of the interface and make a clear distinction between instantaneous interface profiles and the overall, time-averaged, profile which is usually presented. We close with discussion and suggest several routes for future investigations.

II. SIMULATIONS

In this study, we performed extensive simulations of the two-phase atomic crystal-melt system at equilibrium. In all cases, the direction of growth was perpendicular to the face-centered-cubic (fcc) (100) surface. Interatomic interactions were modeled by the Lennard-Jones potential, so that all properties will be presented in Lennard-Jones units (i.e., ϵ for unit energy, σ for unit length, and $\sqrt{m\sigma^2/\epsilon}$ for unit time). In our previous paper[12] the equilibrium temperature for this system was estimated to be $T^{\mathrm{eq}}=0.6972\ \epsilon/k_B$ at a pressure of $P=2.512\times10^{-3}\ \epsilon/\sigma^3$. This is also the state point for our present simulations, which were all carried out at constant number of particles (N), constant volume (V), and constant temperature (T).

The simulations were performed with the DL_POLY package,[15] applying Nosé–Hoover dynamics to keep the average temperature at the desired value. We employed a timestep of $7.480\times10^{-4}\ \sqrt{m\sigma^2/\epsilon}$ and a thermostat relaxation time of $\tau_T=0.0748\ \sqrt{m\sigma^2/\epsilon}$. In Ref. 12 we discussed the tuning of these parameters in detail. The main objective of Ref. 12 was to find bare growth and melting rates, i.e., growth and melting rates for prescribed macroscopic conditions at the interface. In particular this means that, on the microscopic level, nonequilibrium conditions were stationary and homogeneous. For that reason we chose a very stiff thermostat. The thermostat used scales the velocities based on the global temperature so in principle heat-up or cooling-down at the interface could still occur. We checked this by monitoring local averages of the kinetic energy during long production runs and found no noticeable deviation of the interface temperature from the overall temperature. Note that the objective of the present study is to show the equivalence of equilibrium and nonequilibrium simulations. Since we use the same thermostat parameters in both cases a direct comparison should be fully justified.

In the present study two box sizes were investigated: a total of 4048 particles and a total of 8096 particles. In correspondence with our previous study, these sizes will be referred to as the small and the intermediate box size, respectively.

To properly equilibrate the two-phase systems, we started with NVT simulations of bulk liquid (2048 and 4096 particles, respectively) and bulk crystal (2000 and 4000 particles, respectively). Both the liquid and the crystal boxes were constructed with equal cross-sectional areas in the x and y directions (5×5 unit cell lengths) and with elongated axes in the z direction to give the desired equilibrium volumes (at this state point, $v_l=1.1823\ \sigma^3$ and $v_s=1.0414\ \sigma^3$). After 100 000 timesteps of bulk simulations, we wrote configuration files once every 1000 timesteps. From those configuration files, one liquid and one crystal box were set on top of each other (in the z direction) to create two-phase simulation boxes. For both system sizes we thus created four different samples.

In order to release excessive potential energies due to particle overlap in our two-phase system, we performed 300 timesteps of NVT simulations with rigid temperature scaling at every step. Thereafter, 200 000 timesteps of Nosé–Hoover dynamics were carried out before production runs were started. Production runs from which the data in this study were gathered lasted for 20 000 000 timesteps for the small box and 10 000 000 for the intermediate box.

III. CORRELATION BETWEEN PRESSURE FLUCTUATIONS ΔP AND NUMBER FLUCTUATIONS ΔN_s

In this section, we will briefly review the derivation of our 1997 paper[14] [Eq. (10)] and investigate if the factor that contains bulk equilibrium parameters can be replaced by a factor that can readily be obtained from the two-phase simulation. Special attention will be given to the correlation between pressure and number fluctuations and to the difference in decay of the autocorrelation of both of them.

In our earlier paper we introduced an order parameter Ψ to assign particles either to the solid or to the liquid phase. Thus we could, at every instant, calculate the deviations $\Delta N_s=N_s-N_s^{\mathrm{eq}}$ of the number of solidlike particles from their equilibrium value N_s^{eq}. We measured the decay of fluctuations of N_s

$$\langle \Delta N_s(t)\Delta N_s(0)\rangle=\langle \Delta N_s(0)\Delta N_s(0)\rangle \exp\{-t/\tau\}, \qquad (1)$$

which we could relate to the kinetic coefficient k that represents the temperature dependence of growth and melting rates close to equilibrium

$$R(T)=k\frac{\mu_l-\mu_s}{k_BT}\approx -k\frac{h_l^{\mathrm{eq}}-h_s^{\mathrm{eq}}}{k_BT}\frac{\Delta T}{T^{\mathrm{eq}}}. \qquad (2)$$

[Note that in the present study we present growth rates in terms of numbers of particles per unit time, instead of dis-

TABLE I. Thermodynamic data for the bulk Lennard-Jones crystal and liquid. Fits are given for the temperature dependence at constant pressure ($P=2.512\times10^{-3}\ \epsilon/\sigma^3$). See the Appendix for computational details. Values at $T^{\mathrm{eq}}=0.6972\ \epsilon/k_B$ are shown in the second column, and in the last column comparison is made with the thermodynamic data of Johnson (Ref. 18) and van der Hoef (Ref. 19).

$X^{\mathrm{fit}}(T)$	$X^{\mathrm{fit}}(T^{\mathrm{eq}})$	$X^{\mathrm{EoS}}(T^{\mathrm{eq}})$
$v^s=1.0513-0.340\,68\times T+0.468\,30\times T^2$	1.0414	1.0419
$v^l=1.0312-0.158\,02\times T+0.537\,48\times T^2$	1.1823	1.1842
$h^s=-7.6916-0.116\,02\times T+3.2364\times T^2$	−6.199	−6.195
$h^l=-8.313+3.953\times T+0.9729\times T^2$	−5.084	−5.047
$c_v^s=1.132+4.559\times T-3.2554\times T^2$	2.728	2.751
$c_v^l=3.1172+0.750\,39\times T-2.0286\times T^2$	2.654	1.398
$\gamma_V^s=-1.5643+27.041\times T-20.177\times T^2$	7.481	7.665
$\gamma_V^l=11.739-2.1269\times T-7.8532\times T^2$	6.439	5.714
$\kappa_T^s=0.532\,44-1.5627\times T+1.2256\times T^2$	0.038 67	0.039 89
$\kappa_T^l=-0.031\,853+0.076\,666\times T+0.113\,92\times T^2$	0.076 97	0.076 64
$\alpha_P^s=0.266\,16-0.551\,69\times T+0.853\,14\times T^2$	0.2962	0.3058
$\alpha_P^l=-2.1881+7.1913\times T-4.7838\times T^2$	0.5003	0.4380
$\kappa_S^s=\{1/\kappa_T^s+(\gamma_V^s)^2/c_V^s\times vT\}^{-1}$	0.024 54	0.024 64
$\kappa_S^l=\{1/\kappa_T^l+(\gamma_V^l)^2/c_V^l\times vT\}^{-1}$	0.038 66	0.030 93

tance per unit time as in Ref. 14. Therefore the factor A/a in Eqs. (5) and (10) and d in Eq. (12) of that paper will be dropped.]

The basic assumption we make is that number fluctuations ΔN_s induce a volume and consequent pressure change of the crystal and the liquid phase which is instantaneous and homogeneous throughout both phases. In other words, we propose that mechanical equilibrium be reached on a much shorter timescale than the timescale of the crystallization process. The pressure change results in a chemical potential difference between both phases, which acts as the driving force back to equilibrium,

$$\begin{aligned}\frac{d\Delta N_s}{dt}&=\frac{k}{k_BT}(\mu_l-\mu_s)\\&=\frac{k}{k_BT}\left\{\left(\frac{\partial\mu_l}{\partial P}\right)_T^{\mathrm{eq}}\Delta P-\left(\frac{\partial\mu_s}{\partial P}\right)_T^{\mathrm{eq}}\Delta P\right\}\\&=\frac{k(v_l^{\mathrm{eq}}-v_s^{\mathrm{eq}})}{k_BT}\Delta P,\end{aligned}\tag{3}$$

where in the second line we have used the equilibrium condition $\mu_l^{\mathrm{eq}}=\mu_s^{\mathrm{eq}}$.

Now we need a relation between ΔP and ΔN_s, which is provided by the condition of constant total volume,

$$\begin{aligned}V&=(N_l^{\mathrm{eq}}-\Delta N_s)(v_l^{\mathrm{eq}}+\Delta v_l)+(N_s^{\mathrm{eq}}+\Delta N_s)(v_s^{\mathrm{eq}}+\Delta v_s)\\&=(N_l^{\mathrm{eq}}-\Delta N_s)(v_l^{\mathrm{eq}}-v_l^{\mathrm{eq}}\kappa_T^l\Delta P)\\&\quad+(N_s^{\mathrm{eq}}+\Delta N_s)(v_s^{\mathrm{eq}}-v_s^{\mathrm{eq}}\kappa_T^s\Delta P)\\&\approx N_l^{\mathrm{eq}}v_l^{\mathrm{eq}}-N_l^{\mathrm{eq}}v_l^{\mathrm{eq}}\kappa_T^l\Delta P-\Delta N_s v_l^{\mathrm{eq}}+N_s^{\mathrm{eq}}v_s^{\mathrm{eq}}\\&\quad-N_s^{\mathrm{eq}}v_s^{\mathrm{eq}}\kappa_T^s\Delta P+\Delta N_s v_s^{\mathrm{eq}}.\end{aligned}\tag{4}$$

Note that the first line is equivalent to using the classical definition of a Gibbs dividing surface (see also Ref. 7). In the first step we have assumed that both phases respond to the pressure change in the same way as bulk phases. The approximation in the second step is to neglect second-order terms. Now with $V=N_l^{\mathrm{eq}}v_l^{\mathrm{eq}}+N_s^{\mathrm{eq}}v_s^{\mathrm{eq}}$ we find

$$\Delta P=-c\Delta N_s=-\frac{v_l^{\mathrm{eq}}-v_s^{\mathrm{eq}}}{N_l^{\mathrm{eq}}v_l^{\mathrm{eq}}\kappa_T^l+N_s^{\mathrm{eq}}v_s^{\mathrm{eq}}\kappa_T^s}\Delta N_s.\tag{5}$$

This completes the macroscopic law for the decay of number fluctuations

$$\frac{d\Delta N_s}{dt}=-\frac{k}{k_BT}\frac{(v_l^{\mathrm{eq}}-v_s^{\mathrm{eq}})^2}{N_l^{\mathrm{eq}}v_l^{\mathrm{eq}}\kappa_T^l+N_s^{\mathrm{eq}}v_s^{\mathrm{eq}}\kappa_T^s}\Delta N_s.\tag{6}$$

Taking the hypothesis of Onsager[14,16] that "slow fluctuations at equilibrium on average decay according to macroscopic laws" we find, with Eq. (1):

$$\frac{1}{\tau}=\frac{k}{k_BT}\frac{(v_l^{\mathrm{eq}}-v_s^{\mathrm{eq}})^2}{v_s^{\mathrm{eq}}\kappa_T^sN_s^{\mathrm{eq}}+v_l^{\mathrm{eq}}\kappa_T^lN_l^{\mathrm{eq}}}.\tag{7}$$

In our previous study we measured τ in an equilibrium simulation and the kinetic coefficient k derived from it was shown to give good agreement with data from nonequilibrium simulations.

In essence, Eq. (5) is just the statement that an instantaneous correlation exists between ΔN_s and ΔP. Thus, assuming instantaneous linear response, we could also have written

$$\Delta P(t)=\frac{\langle\Delta P(0)\Delta N_s(0)\rangle}{\langle\Delta N_s(0)\Delta N_s(0)\rangle}\Delta N_s(t).\tag{8}$$

The latter expression has the advantage that all the information in it can be taken from one and the same two-phase simulation. No reference has to be made to separate bulk simulations.

In Tables I, II, and III we have listed the relevant bulk data and the factor of Eq. (8). The calculation of the bulk data is described in full detail in the Appendix. The agreement of Eqs. (5) and (8) is very good for both system sizes.

Now we turn to the decay of pressure fluctuations. It is difficult to conceive that an exact *instantaneous* relation exists between pressure fluctuations and number fluctuations. One would rather think that Eq. (5) holds true after averaging over fast fluctuations. As a consequence one may not equate the decay times of $\langle\Delta P(t)\Delta P(0)\rangle$ and $\langle\Delta N_s(t)\Delta N_s(0)\rangle$. To

TABLE II. Results from the fluctuations of N_s and P at equilibrium (NVT) for the small system (4048 particles). The columns show the results after 20 000 000 timesteps of experiments with four different starting configurations.

	(1)	(2)	(3)	(4)
N_s	1764.38	1794.81	1784.39	1776.84
N_l	2283.62	2253.19	2263.61	2271.16
c [Eq. (5)]	0.000 505 26	0.000 508 07	0.000 507 11	0.000 506 41
c (subst. κ_S for κ_T)	0.000 942 67	0.000 946 55	0.000 945 22	0.000 944 25
$\langle \Delta P \Delta P \rangle$	0.006 678 7	0.006 547 7	0.006 371 8	0.006 319 6
$\langle \Delta N_s \Delta N_s \rangle$	8391.6	8187.1	7006.3	7234.5
$\langle \Delta P \Delta N_s \rangle$	−4.8498	−4.6732	−4.1939	−4.4266
$-\langle \Delta P \Delta N_s \rangle / \langle \Delta N_s \Delta N_s \rangle$	0.000 577 94	0.000 570 80	0.000 598 59	0.000 611 87

investigate this point, we write the pressure fluctuation at time t as an instantaneous response to the number fluctuation $\Delta N_s(t)$ (with for the moment an unknown proportionality constant $-c$) plus a random component $\xi(t)$:

$$\Delta P(t) = -c \Delta N_s(t) + \xi(t). \tag{9}$$

Multiplying on both sides with $\Delta P(0)$ and taking the ensemble average gives

$$\begin{aligned}
\langle \Delta P(t) \Delta P(0) \rangle &= c^2 \langle \Delta N_s(t) \Delta N_s(0) \rangle - c \langle \Delta N_s(t) \xi(0) \rangle \\
&\quad - c \langle \xi(t) \Delta N_s(0) \rangle + \langle \xi(t) \xi(0) \rangle \\
&= c^2 \langle \Delta N_s(t) \Delta N_s(0) \rangle - c \langle \Delta N_s(t) \Delta P(0) \rangle \\
&\quad - c \langle \Delta P(t) \Delta N_s(0) \rangle + \langle \xi(t) \xi(0) \rangle \\
&\quad + c \langle (\Delta P(t) - \xi(t)) \Delta N_s(0) \rangle \\
&\quad + c \langle \Delta N_s(t) (\Delta P(0) - \xi(0)) \rangle \\
&= -c \langle \Delta N_s(t) \Delta P(0) \rangle - c \langle \Delta P(t) \Delta N_s(0) \rangle \\
&\quad - c^2 \langle \Delta N_s(t) \Delta N_s(0) \rangle + \langle \xi(t) \xi(0) \rangle \\
&= -2c \langle \Delta P(t) \Delta N_s(0) \rangle \\
&\quad - c^2 \langle \Delta N_s(t) \Delta N_s(0) \rangle + \langle \xi(t) \xi(0) \rangle,
\end{aligned} \tag{10}$$

where in the second step we have substituted Eq. (9). The final step was made on the basis of time symmetry. The accuracy of equating $\langle \Delta P(t) \Delta N_s(0) \rangle$ with $\langle \Delta N_s(t) \Delta P(0) \rangle$ was checked in our simulations and was shown to hold perfectly.

Given the correspondence of Eqs. (5) and (8) that we found above, the best estimate of c would be

$$c = -\frac{\langle \Delta P(0) \Delta N_s(0) \rangle}{\langle \Delta N_s(0) \Delta N_s(0) \rangle}. \tag{11}$$

In Fig. 1 we plotted the various contributions to the pressure fluctuation autocorrelation function, with the above estimated value of c substituted. Clearly, the agreement of the lower two lines is almost perfect. We found that any other value of c gave worse agreement. It is also seen that there is a non-negligible difference between the decay of $\langle \Delta N_s(t) \Delta N_s(0) \rangle$ and $\langle \Delta P(t) \Delta P(0) \rangle$, so that it is not possible to perform an accurate calculation of the kinetic coefficient by using the pressure fluctuations alone. This shows the merits of our solid–liquid discriminator which makes the counting of solid particles possible.

In Fig. 2 we plotted the function $\langle \xi(t) \xi(0) \rangle$. It drops rapidly to very small values, which is not surprising since one expects that the major contribution to ΔP at long times would come from ΔN_s. The function remains fluctuating, however, over a long range of correlation times, much longer than the pressure autocorrelation function in bulk simulations. This is indicative of the fact that ξ does not represent the autonomous pressure fluctuations such as they would occur in a bulk system, but should merely be interpreted as the deviation from an exact instantaneous correlation of ΔP and ΔN_s.

We once more turn to the agreement between Eqs. (5) and (8). One might argue that, although the overall system is thermostatted, local fluctuations can have a distribution different from the canonical one. For instance, if local pressure fluctuations are so fast that no energy transfer is possible, the local subsystem behaves adiabatically and the relation be-

TABLE III. Results from the fluctuations of N_s and P at equilibrium (NVT) for the intermediate size system (8096 particles). The columns show the results after 10 000 000 timesteps of experiments with four different starting configurations.

	(1)	(2)	(3)	(4)
N_s	3579.47	3576.11	3652.22	3597.42
N_l	4516.53	4519.89	4443.78	4498.58
c [Eq. (5)]	0.000 253 80	0.000 253 72	0.000 255 50	0.000 254 22
c (subst. κ_S for κ_T)	0.000 472 95	0.000 472 84	0.000 475 29	0.000 473 53
$\langle \Delta P \Delta P \rangle$	0.003 086 5	0.002 943 6	0.003 118 2	0.002 803 2
$\langle \Delta N_s \Delta N_s \rangle$	13 108	12 292	13 693	10 381
$\langle \Delta P \Delta N_s \rangle$	−3.8981	−3.5878	−4.0642	−2.9783
$-\langle \Delta P \Delta N_s \rangle / \langle \Delta N_s \Delta N_s \rangle$	0.000 297 38	0.000 291 88	0.000 296 81	0.000 286 90

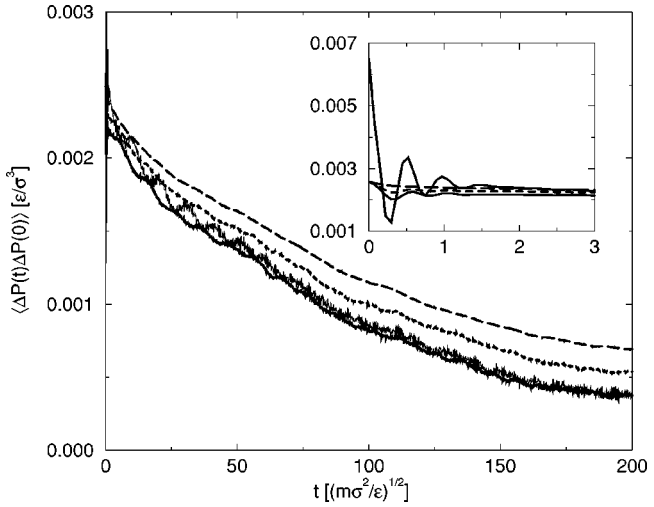

FIG. 1. Autocorrelation of the pressure fluctuations in a small simulation box (4048 atoms). Shown are the various contributions of Eq. (10) from top to bottom: $c^2\langle \Delta N_s(t)\Delta N_s(0)\rangle$ (dashed line); $-c\langle \Delta P(t)\Delta N_s(0)\rangle$ (dotted line); $\langle \Delta P(t)\Delta P(0)\rangle$ (bumpy line); and $-2c\langle \Delta P(t)\Delta N_s(0)\rangle - c^2\langle \Delta N_s(t)\Delta N_s(0)\rangle$.

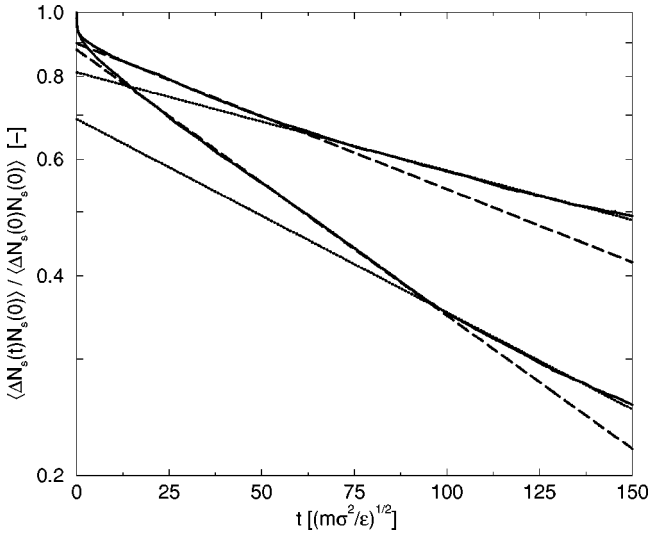

FIG. 3. Fluctuation autocorrelation functions of the amount of solid particles averaged over 4 simulations with 4048 atoms (bottom line) and over 4 simulations with 8096 atoms (top line). Also shown are the fits to the initial regimes (dashed lines) and the long-time regimes (dotted lines).

tween ΔP and Δv would be given by the isentropic compressibility κ_S instead of the isothermal one. For comparison, the factor c of Eq. (5) is also given in Tables II and III with κ_S substituted for κ_T. Clearly, the κ_T expression behaves much better. From this we conclude that at the interface, temperature fluctuations are canonical. This conclusion is justified since we are not looking at the time decay here, but only at the average response of ΔP to ΔN_s.

IV. COMPARISON OF EQUILIBRIUM AND NONEQUILIBRIUM RESULTS

Normalized autocorrelation functions of the number fluctuations [Eq. (1)] were averaged over the four independent experiments (for each box size). The result is displayed in Fig. 3. Clearly, two regimes can be distinguished. To investigate if these regimes can be associated with the regimes of interface relaxation and macroscopic growth—such as they were found in the nonequilibrium simulations—we fitted them to single-exponential functions. Note that the crossover time from the initial to the second regimes is smaller for the intermediate box than for the small box, in accordance with the findings of our previous study.[12] From the relaxation times we calculated kinetic coefficients via Eq. (7), once as it is printed, and once with coefficient c according to Eq. (11).

The results are shown in Table IV, together with the linear coefficients from the fits of Ref. 12 [Eqs. (7) and (8)]. There is some statistical scatter in the data, but the trends for both box sizes are the same.

In Fig. 4, we have plotted the interface relaxation rates as found from the nonequilibrium simulations together with the predicted curves from Table IV. Within the statistical accuracy, the results lie between the linear component of the relaxation rates and the full curve. We conclude that the fluctuations of the interface are such that a substantial part of the nonlinear response is probed by the system. From the figure, it can be roughly estimated that the chemical potential differences associated with fluctuations are equivalent to undercoolings and superheatings of maximum $\pm 0.03\ \epsilon/k_B$. It can also be seen that they do not depend too much on system size. We will come back to this in the next section (Fig. 6).

In Fig. 5 we have plotted the results for the second regime, both from equilibrium and nonequilibrium simulations. The results of both box sizes correspond very well with each other and agree well with the nonequilibrium line. From an analysis of the results for different stages of the run, we found that the statistical uncertainty in the slopes presented in Table IV is of the same order as the difference between the two expressions used. Given the present statistical accuracy, we cannot draw further conclusions as to the validity of Eq. (11).

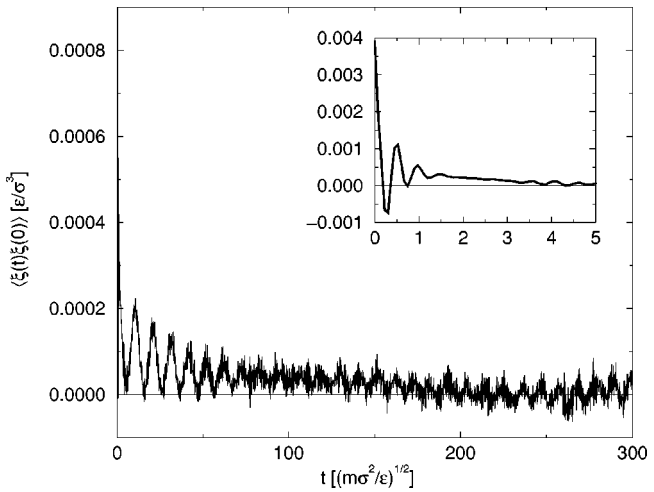

FIG. 2. Autocorrelation of the random component ξ of the pressure fluctuations in a small simulation box (4048 atoms), taken from Eq. (10).

V. THE EQUILIBRIUM INTERFACE

In this section we will take a closer look at the nature of the interface fluctuations at equilibrium. It is generally

TABLE IV. Relaxation times τ and their associated kinetic coefficients as measured from Fig. 3 and Tables II and III. For the small system τ was calculated from fit regions of 10–90 and 90–150 $(m\sigma^2/\epsilon)^{1/2}$, and for the intermediate system from fit regions of 15–60 and 60–150 $(m\sigma^2/\epsilon)^{1/2}$, respectively.

	Interface relaxation	Macroscopic growth
Small system		
τ	108.14	148.70
k [Eq. (7)]	90.304	65.672
k [Eqs. (7) and (11)]	77.582	56.420
$dR/d(\Delta T)$ [Eq. (7)]	−207.14	−150.64
$dR/d(\Delta T)$ [Eqs. (7) and (11)]	−177.96	−129.42
Intermediate system		
τ	197.27	292.63
k [Eq. (7)]	98.631	66.491
k [Eqs. (7) and (11)]	85.537	57.664
$dR/d(\Delta T)$ [Eq. (7)]	−226.24	−152.52
$dR/d(\Delta T)$ [Eqs. (7) and (11)]	−196.21	−132.27
Nonequilibrium results		
$(dR/d(\Delta T))^{eq}$	−184.19	−142.07

known that the Lennard-Jones fcc (100) crystal-melt interface is very diffuse and extends over several interlayer spacings.[7,17] The melting temperature lies well above the thermodynamic roughening transition, which means that growth can occur everywhere on the surface without two-dimensional nucleation barriers. Furthermore, for the fcc (100) surface, all growth sites are equivalent [in contradiction to for instance the (111) surface].

In Fig. 6, we have plotted the distribution of the number of solid particles N_s. The distribution is very smooth with no indication of any preferred numbers. This may serve as evidence that the interface is perfectly rough. Would it have been only slightly faceted, then certain numbers would have shown peaks in the distribution. (Note that the surfaces in both systems contain 50 atoms, so the distribution of N_s represents growth and melting over several layers.) The distribution of N is broader in the intermediate box than in the small box. This is to be expected, since the larger bulk phases in the intermediate box can more easily relax local pressure fluctuations and thus give more ease to fluctuations of the interface. As a consequence, the broadness of any time-averaged interface profile would depend on the overall size of the system, while the local instantaneous interface profile would hardly be affected. The fact that the macroscopic growth rates we found in Fig. 5 are almost independent of system size is a good indication of this point.

In Fig. 7 we have plotted the time-averaged equilibrium profile (over 1 000 000 timesteps) of one interface. Shown are both the density profile and the order parameter profile which is defined (for each histogram bin z_i with a width Δ) as

$$\Phi(z_i)=\frac{1}{A}\left\langle \sum_{k=1}^{N} \Theta(\Psi_k-0.5)\,\delta(z_i-z_k)\right\rangle, \tag{12}$$

with Θ the unit step function, A the cross-sectional area, and δ the discretized delta function, i.e., $\delta(x)=1/\Delta$ for $0<x<\Delta$ and zero otherwise. The order parameter profile represents the counting of liquidlike particles in each bin (cf. the BT profile in Ref. 5, which is essentially the same, but divided by ρ). The order profile coincides with the density of the liquid at the bulk liquid side and would give zero at an ideal crystal side (the little bumps in the crystalline region represent the average amount of imperfections). The order parameter in conjunction with the density profile provides a much more revealing representation of the equilibrium interface than the density alone. We have used the interlayer spacing d as unit on the z axis. It can nicely be seen that, on going from the crystal to the liquid phase, the interlayer spacings gradually grow larger, in good accordance with the results of others.[7,17]

To investigate the instantaneous structure of the interface, we took 5 representative stages in the long (20 000 000

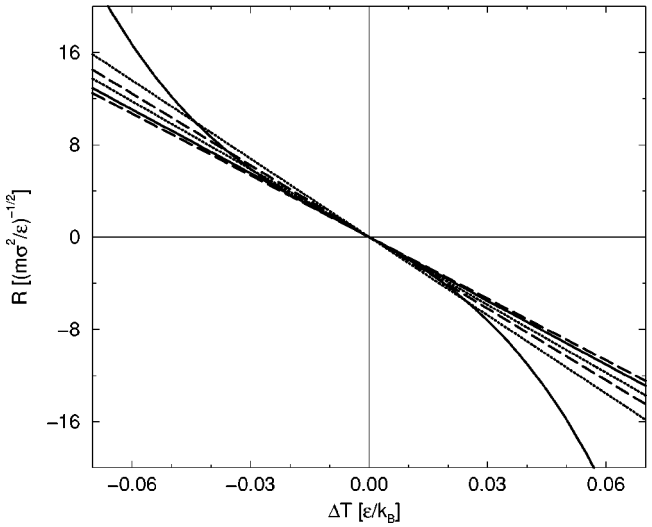

FIG. 4. Interface relaxation rates vs temperature. The curved solid line shows the fit of Ref. 12, the straight solid line shows its linear component. The other lines show equilibrium results for the small box (dashed) and the intermediate box (dotted). For both boxes, the lines with the largest slopes refer to Eq. (7), the others to Eqs. (7) and (11).

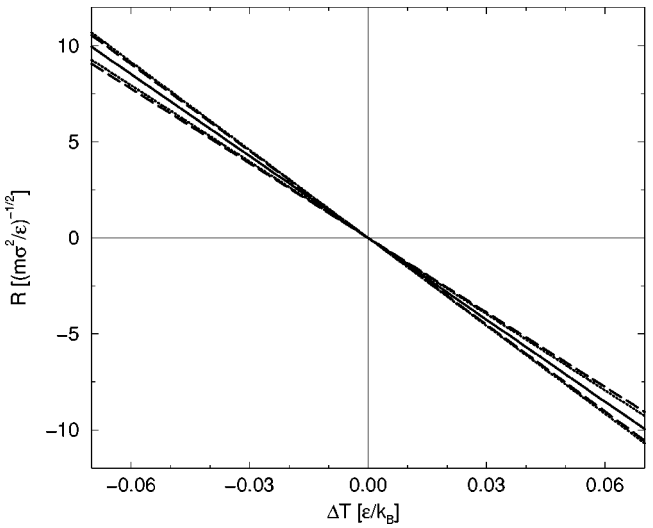

FIG. 5. Crystal growth and melting rates vs temperature. The solid line shows the fit of Ref. 12. The other lines show equilibrium results for the small box (dashed) and the intermediate box (dotted). For both boxes, the lines with the largest slopes refer to Eq. (7), the others to Eqs. (7) and (11).

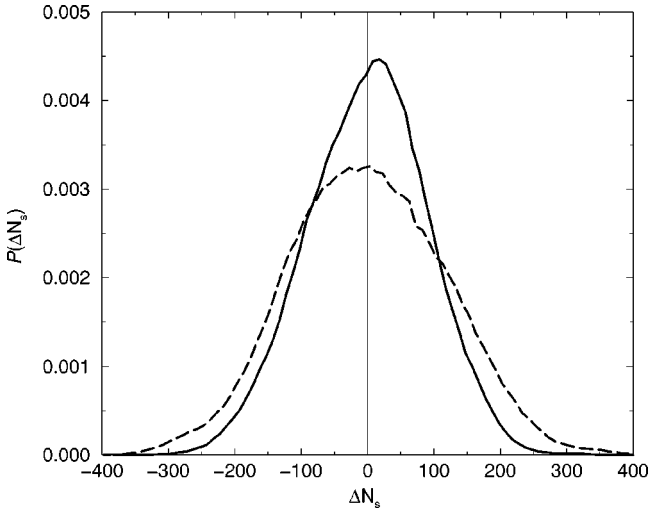

FIG. 6. Equilibrium distributions of the number of solid particles in the small box (solid line) and the intermediate box (dashed line).

timesteps) run of the small box. At each stage, we performed a simulation of 100 000 timesteps and wrote 10 subsequent configurations (one timestep apart) once every 200 timesteps. To obtain sufficient accuracy, the atomic positions of the 10 configurations were averaged and profiles were calculated. We conjecture that these averaged positions are still representative of the instantaneous interface. The profiles were smoothed with a Gaussian filter as follows (see also Hayward and Haymet[6]):

$$\Phi'(z) = \int_{-n}^{n} dz'\, w(z-z')\Phi(z'), \tag{13}$$

with

$$w(z-z') = \frac{1}{\sigma\sqrt{2\pi}} \exp\left(-\frac{1}{2\sigma^2}(z-z')^2 \right), \tag{14}$$

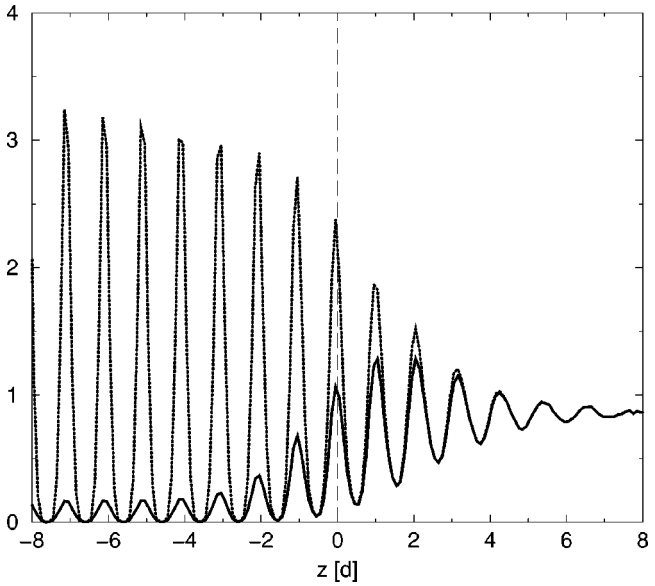

FIG. 7. Time-averaged profiles of the density and the order parameter for the small box, calculated over 1 000 000 timesteps.

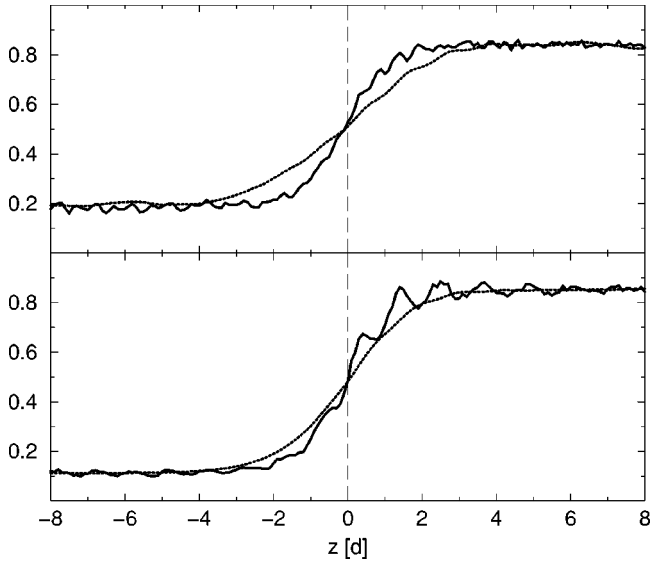

FIG. 8. Time-averaged (dotted lines) and instantaneous (solid lines) interface profiles for the small box (bottom half) and the intermediate box (top half).

where we took the interlayer spacing d as width σ of the Gaussian. The smoothed Φ profiles were then fitted to a tanh function:

$$\Phi^{\mathrm{fit}}(z) = \phi_l[1-f(z)] + f(z)\phi_s, \tag{15}$$

with

$$f(z) = \frac{1}{2}\left[1 - \tanh\left(\frac{z-z_0}{w} \right) \right]. \tag{16}$$

For each 10-step-averaged frame, the position z_0 of the right-hand interface was taken to be the new origin. Profiles (of the right-hand interface) were then constructed on the basis of the atomic positions with respect to this origin. The thus found instantaneous interface profile is plotted in the bottom half of Fig. 8 (solid line). The solid line thus represents the *instantaneous* interface profile, as all interface positions z_0 were put on top of each other.

We also calculated the *time-averaged* profile, i.e., the distribution of the order parameter with respect to the static bulk of the crystal. Since the meaning of this is not trivial, we will explain our procedure. The center of mass of the whole box (liquid+crystal) is conserved in molecular dynamics simulations. We checked that this was indeed the case in our simulations. To study the time-averaged profile of one interface, one might fix, say, the two central planes in the bulk crystal and then measure the fluctuations with respect to their midpoint. But by the conservation of the total center of mass, the fluctuations at one interface would then influence those at the other interface (even if they would be a bulk distance apart). Besides that, fixing crystal planes would introduce an essentially zero Kelvin region in the crystal which is not desirable. Therefore we decided to take as the origin the midpoint of those two bulk crystal layers that were the central layers at the start of the run, without constraining the position of any plane. We found that this midpoint moved a little during the whole run. Particle positions were now binned with respect to the moving origin and the resulting

profiles were averaged over all frames. For comparison with the instantaneous profile, the thus found time-averaged profile was shifted to have its inflexion point at the origin and drawn as the dotted line in Fig. 8. It is shown that the width of the instantaneous interface is smaller than the one of the time-averaged interface.

We repeated the procedure for the intermediate box size (now with 4 runs of 100 000 timesteps), the results of which are shown in the top half of the same figure. The time-averaged profile of the larger box is broader than that of the smaller box (in accordance with the findings of Fig. 5), whereas the widths of the instantaneous profiles are hardly affected by the overall box size.

VI. CONCLUSIONS AND DISCUSSION

We have investigated the performance of a previously introduced method (Ref. 14) to extract the kinetic coefficient for crystal growth from fluctuations in an equilibrium simulation. We applied the method to the same two system sizes that we used in an earlier nonequilibrium study (Ref. 12). We showed that the two regimes that were found previously (an initial regime of interface relaxation and a long-time regime of macroscopic growth) were consistently reproduced by the equilibrium method. This also implies that the same amount of caution must be exercised in calculating growth kinetics from equilibrium simulations as in the nonequilibrium counterpart. In both cases, long runtimes, long observation times, and large box sizes are needed to avoid the confusion of growth rates with interface relaxation rates.

We found that the crossover time between the initial regime and the long-time regime becomes smaller when the size of the system is increased, again in accordance with the nonequilibrium study. This raises the question whether the initial regime would disappear completely in the limit of infinite system size. We interpreted the initial regime to be associated with a relaxation of the equilibrium interface shape to the shape that corresponds to the (nonequilibrium) circumstances of the experiment. If this interpretation is correct, it seems reasonable to conjecture that there must be a size limit where the crossover time levels off, which means that the initial regime should not disappear completely. It would be interesting to further investigate this.

We slightly modified the equilibrium method to incorporate only properties that can directly be evaluated from the two-phase simulation, whereas the earlier approach required external input from separate bulk simulations. Within the statistical accuracy, it was shown that both approaches agree well, although we could not conclude which one of them gives the most reliable results.

With the modification of the method, we found that, on average, a close correlation exists between pressure fluctuations and fluctuations of the amount of crystalline material. We studied the decay of the autocorrelation function of pressure fluctuations and found that, because the above-mentioned correlation is not instantaneous, this cannot be equated to the decay of the autocorrelation function of number fluctuations. The number fluctuations of solid particles $\langle \Delta N_s(t) \Delta N_s(0) \rangle$ provide the most direct route to calculate k from equilibrium simulations.

Finally, we studied the density and order parameter profiles of the equilibrium interface. A clear distinction could be made between the time-averaged overall profile and the average instantaneous profile of the interface, the latter being noticeably smaller. This is of major importance in for example classical density functional theory (DFT) where averaged profiles are mostly used to calculate both energy and entropy contributions to the free energy of the system, whereas it seems reasonable that for energetic considerations the instantaneous profile should be used.

APPENDIX: BULK THERMODYNAMIC PROPERTIES OF THE LENNARD-JONES CRYSTAL AND LIQUID

In this appendix, we will describe how we derived the bulk thermodynamic properties for the Lennard-Jones liquid and fcc crystal as shown in Table I. Most of these could also have been derived from collections (and fits) of thermodynamic data on the Lennard-Jones system by others, the two most recent ones being the Johnson expression[18] (for the liquid) and the van der Hoef expression[19] (for the crystal). The use of these data, however, requires some caution. They represent fits over a limited range of state points and one has to be careful that all state points that one wants to use are covered by the expression. In the following, we will compare our own results with both expressions from the literature.

The procedures for both phases were exactly the same. All liquid calculations were done on a system of 512 particles and all crystal simulations on a system of 500 particles. We used cubic boxes with periodic boundaries. All simulations were run for 5 000 000 timesteps of which 50 000 timesteps were regarded as equilibration and thus disregarded in the evaluations. Nosé–Hoover dynamics were applied with a timestep of $7.480\times10^{-4}\sqrt{m\sigma^2/\epsilon}$ and relaxation times $\tau_T=0.0748\sqrt{m\sigma^2/\epsilon}$ (for thermostatted simulations) and $\tau_P=0.748\sqrt{m\sigma^2/\epsilon}$ (for barostatted simulations).

To obtain the appropriate densities, we started out with NPT simulations at a range of temperatures and at the desired pressure. The average particle volumes are plotted in the top half of Fig. 9. In all figures, the solid lines represent our fits through the data (see also Table I) and the dashed lines represent the expressions of Johnson and van der Hoef. It is clear that the van der Hoef expression describes our results well over the entire range of temperatures. The Johnson expression starts to deviate for lower temperatures. This is not surprising since at that point we enter the metastable liquid region, which is not covered by the data used by Johnson *et al.* Their fit region ranged from $T=0.7$ to $T=2.0$. Our figure clearly shows the danger of extrapolating fitted results out of the fitted region (which becomes even more apparent in the thermodynamic response functions in subsequent figures).

Over the entire temperature range, we subsequently performed NVT and NVE simulations, at the densities that we found with the NPT simulations. In all ensembles, we calculated the average enthalpy per particle h, the results of which are shown in the bottom half of Fig. 9.

For calculating the thermodynamic response functions, we evaluated the average fluctuations of several quantities in

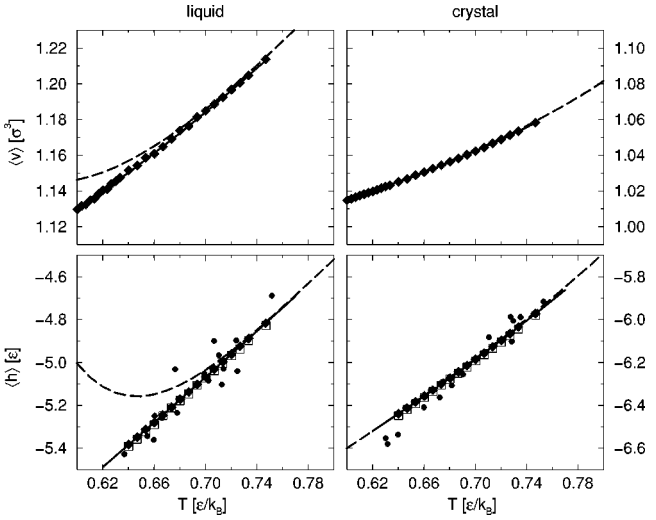

FIG. 9. Enthalpies and volumes per atom vs temperature, as measured from 4950 000 production steps in a bulk liquid (512 atoms) and a bulk crystal (500 atoms) in different ensembles: *NPT* (filled diamonds); *NVT* (open squares); and *NVE* (filled circles). The solid lines represent our fits over the measurement domain (see also Table I). The dotted lines represent the expressions of Johnson (liquid) and van der Hoef (crystal).

our simulations. For a detailed discussion of the use of fluctuation formulas to this end, the reader is referred to the literature.[20–22] The isochoric heat capacity per atom $[c_V = N^{-1}(\partial U/\partial T)_V]$ was calculated from the fluctuations of the total energy and of the potential energy, both in the *NVT* ensemble, and from the fluctuations of the kinetic energy in the *NVE* ensemble:

$$\langle \Delta U \Delta U \rangle_{NVT} = k_B T^2 N c_V, \tag{A1}$$

$$\langle \Delta \Phi \Delta \Phi \rangle_{NVT} = k_B T^2 \left(N c_V - \frac{3}{2} N k_B \right), \tag{A2}$$

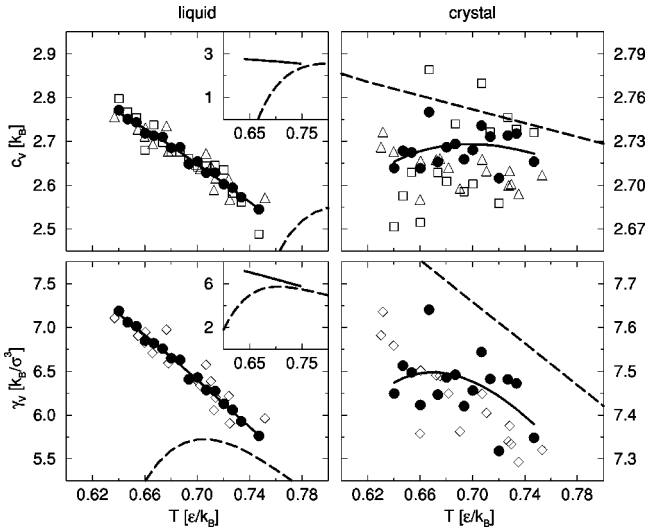

FIG. 10. Isochoric heat capacity and thermal pressure coefficient vs temperature in a bulk liquid and a bulk crystal. Symbols denote results from Eqs. (A2) (filled circles, solid line shows fit), (A1) (open squares), (A3) (open triangles), (A4) (filled circles, solid lines show fits), and (A5) (open diamonds). Dashed lines represent the expressions of Johnson (liquid) and van der Hoef (crystal).

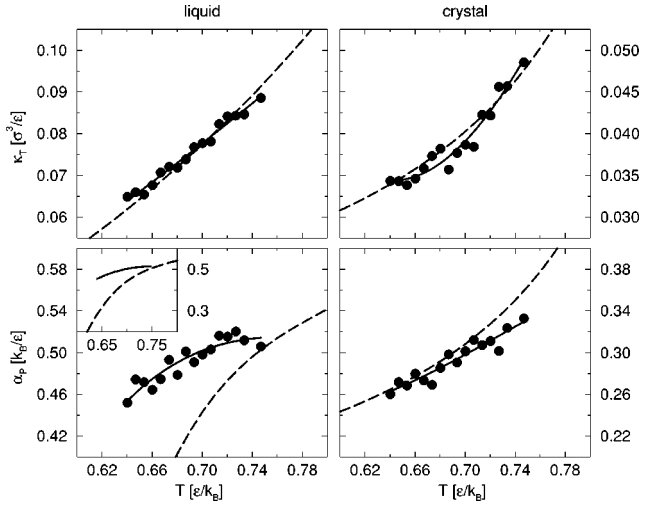

FIG. 11. Isothermal compressibility and thermal expansion coefficient vs temperature in a bulk liquid and a bulk crystal. Symbols denote results from Eqs. (A4) (filled circles, solid lines show fits), (A5) (open diamonds), and (A7) (filled circles, solid line shows fit). Dashed lines represent the expressions of Johnson (liquid) and van der Hoef (crystal).

$$\langle \Delta \hat{T} \Delta \hat{T} \rangle_{NVE} = \frac{3}{2} N k_B^2 T^2 \left(1 - \frac{3 N k_B}{2 N c_V} \right). \tag{A3}$$

The results are shown in Fig. 10. Clearly, Eq. (A2) gives the best statistics, so that data were used for the fit.

The thermal pressure coefficient $(\gamma_V = (\partial P/\partial T)_V)$ was calculated from

$$\langle \Delta \Phi \Delta \hat{P} \rangle_{NVT} = k_B^2 T^2 (\gamma_V - \rho k_B), \tag{A4}$$

$$\langle \Delta \hat{P} \Delta \Phi \rangle_{NVE} = \frac{N k_B^2 T^2}{V} \left(1 - \frac{3 V \gamma_V}{2 N c_V} \right), \tag{A5}$$

the results of which are also plotted in Fig. 10. Given the small variations of both c_V and γ_V for the crystal over this temperature range (see the scale in the figures), the van der Hoef expression gives satisfactory results. The Johnson expression seems to be way off for both properties, but the insets in the figures show that the data converge to the expression just above $T = 0.7$.

Finally, the isothermal compressibility $[\kappa_T = -V^{-1}(\partial V/\partial P)_T]$ and the thermal expansion coefficient $[\alpha_P = V^{-1}(\partial V/\partial T)_P]$ were calculated with

$$\langle \Delta V \Delta V \rangle_{NPT} = V k_B T \kappa_T \tag{A6}$$

and

$$\langle \Delta V \Delta (U + \hat{P} V) \rangle_{NPT} = k_B T^2 V \alpha_P . \tag{A7}$$

Results for the latter two properties are shown in Fig. 11.

Adams[23] has emphasized that when fluctuation formulas such as the above are used in a computer simulation, it is advisable to crosscheck them with the thermodynamic identity $\alpha_P = \kappa_T \gamma_V$. A quick check with the equilibrium values in Table I shows that the agreement is good.

[1] K. A. Jackson, J. Cryst. Growth **198/199**, 1 (1999).
[2] B. B. Laird and A. D. J. Haymet, Chem. Rev. **92**, 1819 (1992).
[3] A. C. Levi and M. Kotrla, J. Phys.: Condens. Matter **9**, 299 (1997).
[4] R. L. Davidchack and B. B. Laird, J. Chem. Phys. **108**, 9452 (1998).

[5] B. J. Jesson and P. A. Madden, J. Chem. Phys. **113**, 5935 (2000).
[6] J. A. Hayward and A. D. J. Haymet, J. Chem. Phys. **114**, 3713 (2001).
[7] H. E. A. Huitema, M. J. Vlot, and J. P. van der Eerden, J. Chem. Phys. **111**, 4714 (1999)
[8] C. J. Tymczak and J. R. Ray, Phys. Rev. Lett. **64**, 1278 (1990).
[9] C. J. Tymczak and J. R. Ray, J. Chem. Phys. **92**, 7520 (1990).
[10] G. Tammann, *Aggregatzustände. Die Zustandsänderungen der Materie in Abhängigkeit von Druck und Temperatur* (Leopold Voss, Leipzig, 1923), Chap. 9.
[11] D. R. Uhlmann, J. F. Hays, and D. Turnbull, Phys. Chem. Glasses **8**, 1 (1967).
[12] H. L. Tepper and W. J. Briels, J. Chem. Phys. **115**, 9434 (2001).
[13] H. L. Tepper and W. J. Briels, J. Cryst. Growth **230**, 270 (2001).
[14] W. J. Briels and H. L. Tepper, Phys. Rev. Lett. **79**, 5074 (1997).
[15] W. Smith and T. R. Forester, J. Mol. Graphics **14**, 136 (1996).
[16] D. Chandler, *Introduction to Modern Statistical Mechanics* (Oxford University Press, Oxford, 1987), Chap. 8.
[17] E. Burke, J. Q. Broughton, and G. H. Gilmer, J. Chem. Phys. **89**, 1030 (1988).
[18] J. K. Johnson, J. A. Zollweg, and K. E. Gubbins, Mol. Phys. **78**, 591 (1993).
[19] M. A. van der Hoef, J. Chem. Phys. **113**, 8142 (2000).
[20] M. P. Allen and D. J. Tildesley, *Computer Simulation of Liquids* (Oxford University Press, Oxford, 1987).
[21] M. P. Allen, in *Computer Simulation in Chemical Physics*, edited by M. P. Allen and D. J. Tildesley (Kluwer Academic, The Netherlands, 1993), pp. 49–92.
[22] A. A. Gusev, M. M. Zehnder, and U. W. Suter, Phys. Rev. B **54**, 1 (1996).
[23] D. J. Adams, Mol. Phys. **29**, 307 (1975).